JOURNAL OF AIRCRAFT
Vol. 43, No. 5, September–October 2006

Joined-Wing Sensor-Craft Configuration Design

Cody C. Rasmussen* and Robert A. Canfield†
U.S. Air Force Institute of Technology, Wright–Patterson Air Force Base, Ohio 45433-7765
and
Maxwell Blair‡
U.S. Air Force Research Laboratory, Wright–Patterson Air Force Base, Ohio 45433-7542

DOI: 10.2514/1.21951

An optimized configuration design using both structural and aerodynamic analyses of a joined-wing configuration is presented here. The joined-wing aircraft concept fulfills a proposed long-endurance surveillance mission and incorporates a load-bearing antenna structure embedded in the wing skin. A range of joined-wing configurations were trimmed for critical flight conditions and then structurally optimized for trimmed flight and gust loads to achieve a minimum weight for each single configuration. A response surface statistical analysis was then applied to determine optimized joined-wing aircraft configurations. The optimal configurations were then reanalyzed and verified by examining nonlinear structural deflection characteristics and analyzing material and aerodynamic distributions.

Nomenclature

C_i	=	coefficient for curve/surface fit
c_m	=	chord at intersection
c_{ra}	=	chord at aft wing root
c_{rf}	=	chord at front wing root
c_t	=	chord at outboard wing tip
E_x	=	Young's modulus of elasticity in x direction (primary ply direction)
E_y	=	Young's modulus of elasticity in y direction (secondary ply direction)
G_{xy}	=	modulus of rigidity
K	=	gust alleviation factor
S_{ib}	=	span length from wing root to end of joint wing section
S_{ob}	=	span of outboard wing section
t	=	skin thickness
t_{ply}	=	thickness per composite ply
t/c	=	thickness-to-chord ratio
U_g	=	vertical gust velocity
V	=	vehicle velocity
w	=	fitted vehicle weight value
x_i	=	configuration design variable
z_{fa}	=	vertical offset
$\Delta\alpha$	=	change in angle of attack
$\varepsilon_{\text{yield}}$	=	strain value at material yield
$\varepsilon_{\text{yield safety}}$	=	strain value at factor of safety with respect to yield
Λ_{ib}	=	front wing sweep angle
Λ_{ia}	=	aft wing sweep angle
Λ_{ob}	=	outboard wing sweep angle
$\mu\varepsilon$	=	microstrain
ν_{xy}	=	Poisson's ratio
ξ	=	normalized span distance

Presented as Paper 1760 at the 45th AIAA/ASME/ASCE/AHS/ASC Structures, Structural Dynamics, and Materials Conference, Palm Springs, California, 19–22 April 2004; received 21 December 2005; revision received 14 February 2006; accepted for publication 14 February 2006. This material is declared a work of the U.S. Government and is not subject to copyright protection in the United States. Copies of this paper may be made for personal or internal use, on condition that the copier pay the $10.00 per-copy fee to the Copyright Clearance Center, Inc., 222 Rosewood Drive, Danvers, MA 01923; include the code $10.00 in correspondence with the CCC.

*Graduate Student, Department of Aeronautics and Astronautics; cody.rasmussen@afit.edu. AIAA member.
†Associate Professor, Department of Aeronautics and Astronautics; robert.canfield@afit.edu. Associate Fellow AIAA.
‡Research Engineer, Air Vehicles Directorate; maxwell.blair@wpafb.af.mil. Associate Fellow AIAA

I. Introduction

SENSOR craft is a conceptual aircraft based on an Air Force need for advanced, long-endurance tactical surveillance using current and future sensor packages. A potential vehicle design is a joined-wing configuration that could lead to improved radar capabilities, increased aerodynamic performance, and structural weight savings.

Recent work included completing a series of structural and aerodynamic simulations for a single configuration joined-wing design. Using that process, simulations were conducted on a range of configurations instead of a single configuration baseline configuration. This provided a greater understanding of static aeroelastic response to joined-wing configuration changes.

Recent analyses have shown that an example joined-wing configuration exhibits large geometric nonlinearity below the critical buckling eigenvalue. Nonlinear analysis was critical to correctly model some, if not all, sensor-craft configurations. In addition, it has been shown that buckling is a critical constraint. This new study involved a gradient-based weight-optimized design that was buckling safe and did not exceed fiber strain limits.

The optimization was two tiered. The first tier included finding a minimum weight for each configuration through structural optimization. For each geometric aircraft configuration, a set of structural and aerodynamic analyses were completed and combined to provide a total mission load history. A weight-optimized solution was found by varying spar, rib, and skin thicknesses of the wing structure. This paper focuses on the single configuration optimization process.

The next level of optimization included using an approximation method covering the entire design space. This was achieved by creating a response surface from 74 data points obtained from the single configuration optimization process. The main goal of this study was to obtain general relationships between each joined-wing configuration design variable. The details of the multiple configuration design and optimization process are provided in an additional paper [1].

Four different critical mission points were analyzed for each particular configuration. The mission load sets were combined to form a complete structural analysis over which aircraft weight was minimized for the total mission range.

This sensor-craft analysis and design used radar transmissive material in the analysis. A conformal load bearing antenna structure (CLAS), consisting of graphite-epoxy composite, carbon foam core,

and cyanite ester (Astroquartz) materials, was used throughout the aft and front wing skins.

II. Background

Wolkovich proposed a joined-wing design with potential weight savings and aerodynamic benefits as early as 1986 [2]. He pointed out the inclined plane of the joined wing will cause a forward bending moment about the vertical axis. To counter this bending moment, Wolkovich stated that the structural material distribution should be as far away from the inclined bending plane as possible [2]. This requires that the upper leading edge and lower trailing edge of a joined wing contain the most structural material possible.

Gallman and Kroo examined a joined-wing configuration to meet the mission requirements of a medium-range transport aircraft [3,4]. They used a simplified aluminum wing box structure in the finite element model. This simplified model was optimized for a minimum weight under gust load conditions. They used zero fuel weight due to the increased load factor caused by a gust under this flight condition. When Gallman and Kroo included buckling as a design constraint in their analysis, the weight increased by 13%. This led to a higher direct operating cost when compared to a Boeing 727. However, they conceded, "a different set of mission specifications and design assumptions may produce joined wings that perform significantly better" [3]. This current research includes gust loads as well as taxi-crater impact, landing, and steady maneuver load cases.

In 1984, the NASA Ames Research Center began a study to research the possibility of building a joined-wing airplane. NASA intended the aircraft to be a proof-of-concept demonstrator. The researchers discovered that even with extensive aerodynamic design, the wind tunnel model still exhibited an unstable stall characteristic [5]. The stall characteristic was improved with vortilions installed on the wind tunnel model. It should be noted that there was no structural optimization design performed. The horizontal tail structure was strengthened with additional material where buckling was predicted [6,7].

Extending research on the NASA Ames feasibility study, Lin et al. examined the joint configuration with the NASA wind tunnel model [8]. They employed linear FEM analysis and experimental analysis on the wind tunnel model. The NASTRAN analysis indicated a lower root bending moment than the experimental results. They concluded that the rigid wing joint had the best structural characteristics. The current sensor-craft configuration assumes the use of a rigid joint configuration. The current structural model also includes a preliminary concept of the rib and spar configuration at the wing joint.

Livne surveyed past joined-wing research and attempted to provide a direction for future studies [9]. He concluded the joined-wing configuration creates complex interactions between aerodynamics and structures. Livne advocated the use of a multidisciplinary design approach to simultaneously design aerodynamics and structures. This study integrated structural and aerodynamic design into a single process.

Blair and Canfield proposed an integrated design method for joined-wing configurations [10]. Blair developed a geometric model and user interface using the Adaptive Modeling Language. The model can be analyzed for structural or aerodynamic characteristics through external software. They concluded that nonlinear structural analysis is important to accurately capture the large deformations that occur in this joined-wing configuration [11].

Recent work conducted by Roberts et al. included a single-point configuration design of a joined wing that was weight optimized using a nonlinear analysis with implicit buckling constraints [11]. For a structurally optimized configuration under linear analysis, nonlinear deformations were found to be over 10 times as great for an aluminum joined-wing structure [11]. This current research expands and automates this analysis and weight optimization process to facilitate the process of conducting multiple analyses on multiple configurations. This will provide understanding into aeroelastic effects for various configuration changes.

Weisshaar and Lee explored configuration changes of a joined-wing aircraft with respect to flutter speed using Rayleigh–Ritz modeling [12]. The most noteworthy results related to joint location and sweep angle. They examined sweep angles from 30 to 45 deg using parametric methods. In general, as the sweep angle rose for a fixed span size, the flutter dynamic pressure increased. In addition, as the joint location moved closer to the tip of the wing, the flutter dynamic pressure decreased slightly. This current research explored parametric configuration changes like Lee, except it was optimized for flexible static air loads and global buckling instead of conducting a flutter analysis.

Nangia et al. analyzed the effects of forward swept outboard wings on a joined-wing aircraft [13]. They found that a forward swept outboard wing produces favorable lift distribution on the forward and aft wings through a forward placement of the center of pressure for the overall aircraft vehicle. The current approach led to a similar result. The optimum configuration in Sec. IV has a forward swept outboard wing.

III. Optimization Design Process

A. Aircraft Geometry Configuration Variables

Each geometric configuration was defined by six key independent design variables. From these variables and from a set of equality constraints, each geometry fixed joined-wing configuration was determined. Figure 1 depicts a typical joined-wing planform configuration used in this study, and Table 1 lists the relevant geometric variables used to determine the range of configurations.

Three separate sweep angles were used to define wing geometry. The front wing sweep angle involved changing the wing angle of the front wing joint incident with the fuselage centerline. The outboard wing sweep angle varied the angle of the wing part that extends from the joint to the tip. The aft wing sweep angle defined the angle the aft wing creates with the fuselage. For configuration consistency, the span $(S_{ib} + S_{ob})$ was set constant. The joint location $[S_{ib}/(S_{ib} + S_{ob})]$ involved varying the intersect point where the front wing coincides with the aft wing. The vertical offset of the aft wing intersection to fuselage was the vertical distance between where the aft wing root is connected to the vertical tail wing and where the front wing connects to the fuselage. Finally, the thickness-to-chord ratio of a standard airfoil was varied to represent actual geometric changes in wing box size (vertical stretch of airfoil). All chord lengths were set constant to meet requirements of a radar array imbedded in the wing.

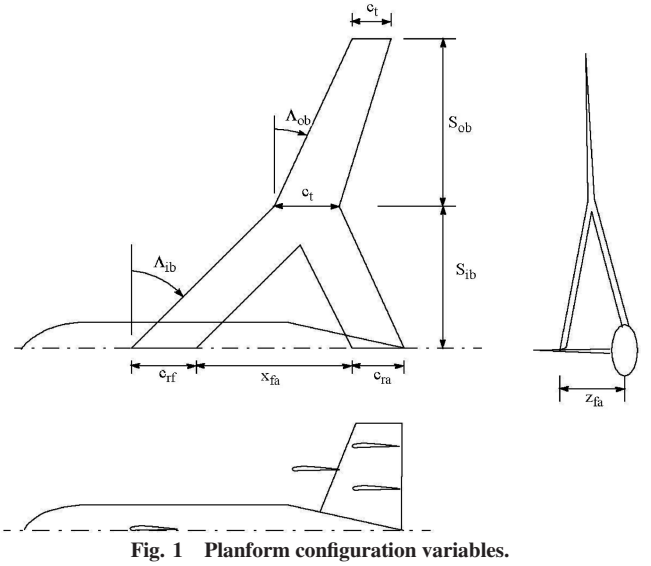

Fig. 1 Planform configuration variables.

Table 1 Baseline configuration parameters [6]

Variable	Name	Size
$S_{ib}/(S_{ib} + S_{ob})$	Joint location	Varies
$S_{ib} + S_{ob}$	Total span length	32.25 m
Z_{fa}	Vertical offset	Varies
Λ_{ib}	Front wing sweep	Varies
Λ_{ia}	Aft wing sweep	Varies
Λ_{ob}	Outboard wing sweep	Varies
c_{rf}	Chord at front root	2.50 m
c_{ra}	Chord at aft root	2.50 m
c_m	Chord at intersection	2.50 m
c_t	Chord at tip	2.50 m
t/c_i	Thickness/chord	Varies

B. Upper and Lower Bound Constraints

Each of the six key design variables had a defined range where it was feasible. This limited the analysis to reside within a reasonable scope.

The front and aft wing sweep angles were constrained by the system's radar coverage requirements. The radar transmissive material contained within the wings must provide 360 deg of coverage around the vehicle. The maximum change in the electromagnetic beam steering angle from the normal direction of the wing at which the end-fire radar can properly receive/transmit is approximately 60 deg, also known as the grazing angle. This implies that the front and aft wings must have a sweep angle within 30–60 deg to achieve complete coverage. For configuration exploration, the aft wing was allowed to have 0 deg sweep to create a center of gravity that was more forward than aft. There is an aerodynamic penalty for a wing sweep greater than 30 deg. However, for an exploration study such as this, large wing sweep angles were investigated so this study would not be overconstrained.

The horizontal distance between the forward and aft wing roots was not an independent design variable for this problem because both the front and aft sweep angles defined this as horizontal offset distance. In addition, the outboard wing sweep angle ranged from -30 deg to a maximum of 60 deg.

The vertical offset of the root location of the front and aft wings ranged from 0.0 to 10 m. A vertical offset of 0.0 m defined a front and an aft wing within the same horizontal plane. This prevented the aft wing from residing lower than the front wing. An offset of 10 m kept the vertical offset from growing to the extent that the vertical tail becomes so large that the fuselage weight assumption should be considered false.

The fractional joint location ranged from 0.5 to 0.9. At 1.0, the aft wing and the front wing are joined at the tip. A maximum joint location of 0.9 was used such that an outboard wing will exist for every configuration. A joint location less than 0.5 was not used. This left enough room for the radar array to reside within the front and aft wings.

The thickness-to-chord ratio ranged from 0.106 to 0.20. Because the wings were offset, the twisting and bending moments of inertia were atypical. Thin t/c ratios proved to be more lightweight overall, because the bending axis is tilted, not horizontal.

Table 2 lists all upper and lower bounds for each design variable. Figure 2 shows a sketch of each configuration when each design variable is set at its lower and upper bounds and its midrange.

Table 2 Design variable bounds

Variable	Variable description	Lower bound	Upper bound
t/c	Thickness/chord	10.6%	20%
$S_{ib} + S_{ob}$	Joint location	0.5	0.9
Z_{fa}	Vertical offset	0.0 m	10 m
Λ_{ib}	Front wing sweep	30°	60°
Λ_{ia}	Aft wing sweep	0°	60°
Λ_{ob}	Outboard wing sweep	0°	60°

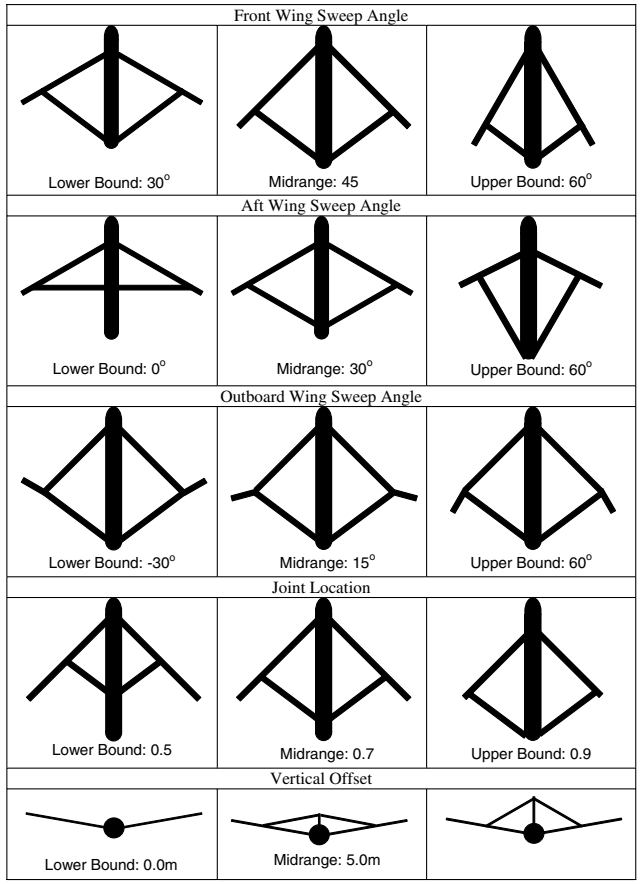

Fig. 2 Sketches of joined-wing configuration ranging through each design variable.

C. AVTIE Model and Environment

The Adaptive Modeling Language (AML), developed by TechnoSoft, Inc., allows a researcher to develop a model with customized geometric relationships [14]. Blair and Canfield developed the Air Vehicles Technology Integration Environment (AVTIE) [10] which provided a user interface to the AML software capabilities. AVTIE converted the geometric model into data files which were manipulated into a complete NASTRAN optimization run. The six key geometric configuration variables were entered into the AVTIE interface to create unique NASTRAN grid points for various configurations used in this study.

D. Mission Cases

Four critical load sets were used for a gradient-based design method using MSC.NASTRAN [15]. Aerodynamic load sets were obtained from MSC.FlightLoads [16,17] for each respective mission category. Appropriate fuel weight forces were applied for percent mission complete. The fuel forces were originally created within the AVTIE interface. The fuel was assumed to be carried in the wings and was scaled for the aircraft's weight for every aircraft configuration. The taxi impact load case is a nonaerodynamic load set which only factors fuel weight [18]. Gust loads were created using a calculated change in the angle of attack induced by the gusts

Table 3 Mission load sets [11]

Load type	Mission category	Mission complete
Maneuver	Ingress	0%
Maneuver	Egress	98%
Turbulent gust	Egress	98%
Taxi impact	Preingress	0%

$$\Delta\alpha = \frac{KU_g}{V} \tag{1}$$

where $\Delta\alpha$ is due to the gust, and V is the velocity of the aircraft [19]. The $\Delta\alpha$ was then applied to the FlightLoads model to generate proper static instantaneous gust loads. The highlighted mission loads in Table 3 are the applied critical mission sets used in the configuration analysis.

E. Step 1: Independent Configuration Weight Minimization Process

The joined-wing configuration was optimized in three phases. Each joined-wing configuration was optimized individually in every phase. Each phase contained a NASTRAN optimization based on a FlightLoads analysis that was integrated through MatLab [20].

The first phase included standard FlightLoads trim data for maneuver loads and vehicle weight accounting for impact load sets. Buckling loads generated from a sample PanAir model were applied in the first run for initial estimate purposes only.

The second phase included the same maneuver static trim and impact load sets as in phase one, except the static trimmed forces from the maneuver loads contained in the first run were also applied as static load sets for buckling analysis. In addition, changes in angles of attack for the instantaneous gust cases were calculated and then applied in phase two to determine the associated gust loads.

Phase three included static aerodynamic analysis for maneuver loads, instantaneous gust loads from phase two, and impact loads from fuel weight. The maneuver and gust loads from phase two were applied in phase three's buckling analysis. The three phase process is shown in Fig. 3.

Element displacements and stresses due to the load conditions were computed in NASTRAN. Both a strain and buckling analysis were used as constraints within the NASTRAN optimization. The NASTRAN optimizer resized each element to provide the minimum weight using a gradient-based design. Constraints were applied to all elements to have a 1.5 factor of safety applied to the allowable fiber strain and a buckling limit load of 1.5 times the design load. Table 4 shows the graphite epoxy material properties.

Long run times were found to occur in NASTRAN optimization and in the trimming process using AVTIE. Run times were reduced through the use of FlightLoads for trimmed loads and the use of polynomial curve fits for the material distribution. FlightLoads is an integrated element with the NASTRAN optimization analysis. This reduced computation time significantly. FlightLoads was used to trim the aircraft with linear transpiration boundary conditions. Thus, follower forces were not considered in this optimization process.

Because the original NASTRAN design model included over 22,800 thickness design variables, a design space reduction was employed. The structural shell thickness variables were estimated in terms of independent variables in the form of polynomial curve fits where ξ was the spanwise location of the designable element. Cubic

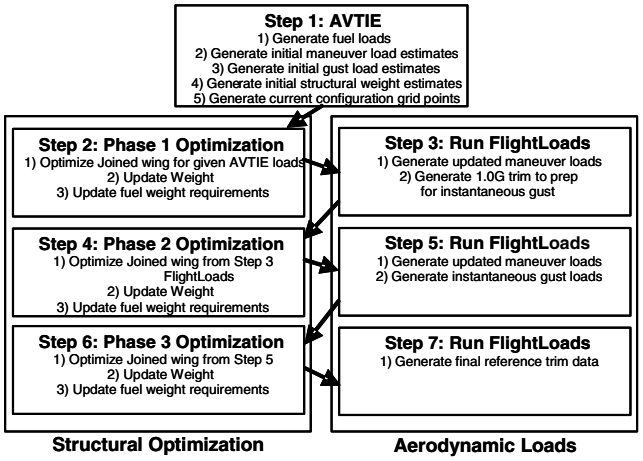

Fig. 3 Single configuration phasing process (integration between FlightLoads and NASTRAN).

Table 4 Graphite epoxy: IM7/977-3 material properties [11]

Property	Value
E_x	1.53E + 11 Pa
E_y	1.48E + 11 Pa
ν_{xy}	0.3
G_{xy}	4.14E + 9 Pa
t_{ply}	0.142 mm
$\varepsilon_{\text{yield}}$	0.00500 $\mu\varepsilon$
$\varepsilon_{\text{yield safety}}$	0.00300 $\mu\varepsilon$

basis functions composed of user-defined design variables resized each element within the wing-box structure:

$$C_0 + C_1\xi + C_2\xi^2 + C_3\xi^3 = t_i \tag{2}$$

The curve fits were separated by part location. The front wing, aft wing, outboard wing, and joint wing segments were designed separately. Within each of these wing segments, each spar was designed with its own cubic basis function. Additionally, all the ribs within each wing segment were designed with its own respective function. Finally, spanwise strips within the wing skins were designed separately and controlled by different cubic basis functions. The total number of independent design variables was reduced to 512 by using a third order polynomial curve fit and separate designable regions. The differently designable areas within the wing skins are displayed in Fig. 4.

F. Step 2: Multiple Configuration Weight Minimization Process

To find optimal joined-wing configurations and configuration design trends, a design of experiments, or rather a sampling space,

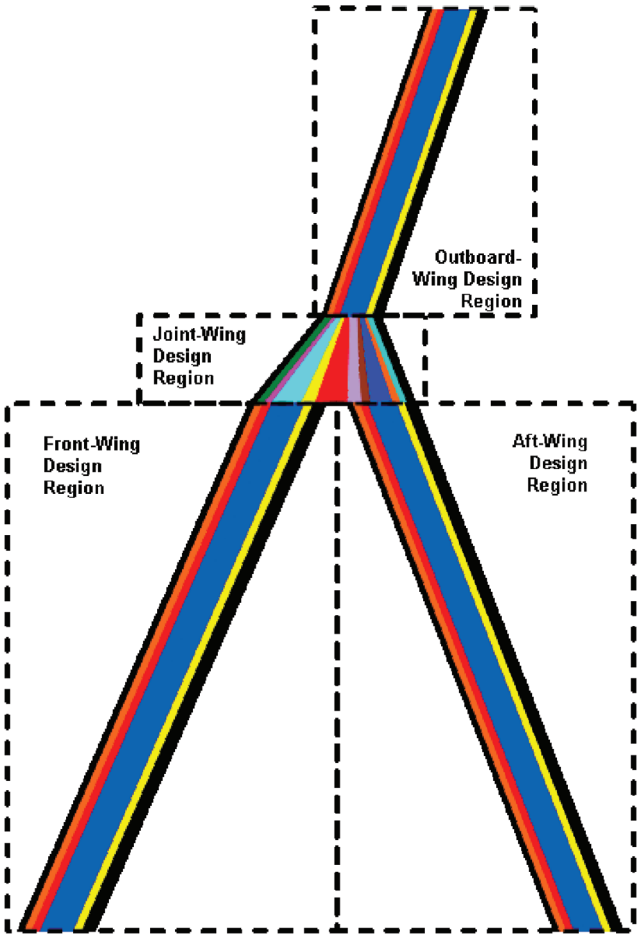

Fig. 4 Regions of common cubic basis functions for skin thickness sizing: top view.

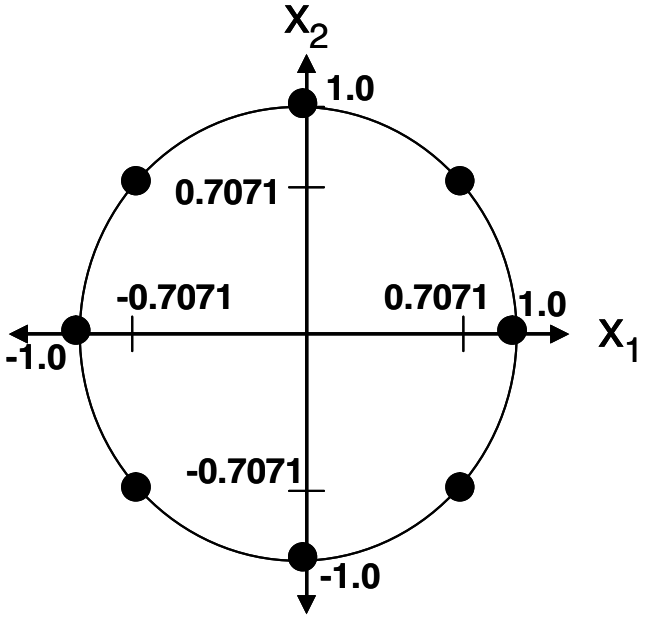

Fig. 5 Sampling space for a two design variable combination.

was established. The design trends and relationships were explored through a response surface fit of the sampled single optimized joined-wing configurations. Classical function minimization techniques were then used on the response surface to determine optimal regions of the surface. The optimal regions defined general joined-wing configuration characteristics for a lightweight aircraft.

Taking the set of minimized weights for 74 joined-wing configurations, a function in terms of the configuration design variables was created using response surface methodology:

$$w = C_0 + \sum_{i=1}^{6} C_i X_i + \sum_{i=1}^{6} \sum_{j=1}^{6} C_{ij} X_i X_j \tag{3}$$

From this function, with its determined coefficients, classical minimization optimization techniques were used to extrapolate an optimized configuration solution.

The main goal of this study was to obtain general relationships between each configuration design variable. A total of 15 relationship combinations exist for six independent design variables where only a maximum of two design variables were compared for each combination. For example, the front wing sweep angle was compared to the aft wing sweep angle, the outboard wing sweep angle, the joint location, the thickness-chord ratio, and the vertical offset. This was completed for every configuration design variable combination.

Four sample configuration points were taken for each combination for a total of 60 response surface data points. The four data points were 70.7% of the maximum and 70.7% of the minimum of each variable in each two variable combination. Additionally, each variable was sampled at 100% of its maximum and minimum. In addition, two baseline configurations were analyzed which resulted in a total of 74 total data points to create the final response surface. Figure 5 shows the sampling space of a two design variable combination where only two design variables vary while the other four key configuration variables remain at their midpoint (between the variable's lower and upper bounds).

IV. Results

A. Optimal Region

Classical minimization techniques were applied to the response surface. Since negative curvature exists in the response surface, the starting point will affect which of several local optimal points the optimizer will converge to. Because the response surface was a second order function, the optimizer can only get "stuck" at boundaries or at an interior local minimum. To avoid finding only one optimal point in the surface, all possible upper and lower bound combinations of the six key configuration design variables were used as starting points. Only three unique optimal points were found. Table 5 shows the variable values and the fitted weight for these three optimal configurations.

The fitted weight values were found to be negative. This shows that the response surface poorly fits the data in some regions. Overall, the R^2 value of 0.853 only indicates a moderately good fit. Thus, the response surface was only used to identify optimal regions, not to determine precise optimal joined-wing configurations. All three approximate optimal configurations were then reoptimized to find their true weight values (observed weights). This showed that the lowest fitted weight configuration (Fig. 6) was not the same as the lowest observed weight configuration (Fig. 7). Because the initial response surface exhibited negative weight values, a new response surface was generated with the addition of the three new optimal weight samples.

With the additional optimal configuration weight values, the response surface did not display negative values across the design space. Moreover, the lowest fitted weight configuration (Fig. 6) did not exhibit a typical outboard wing sweep angle. To explore this phenomenon, the same configuration was reoptimized with an outboard wing sweep of 0 deg. The observed optimized weight was 2920.4 kg, a reduction of almost 1000 kg. This reinforces the conclusion that the response surface is only moderately fit. The other optimal regions need adaptive refinement for better accuracy in converging to the actual optimal configuration. The current result, from the first coarse iteration, merely indicates trends.

The most significant differences between the two optimal configurations of interest are the changes in outboard wing sweep angle, airfoil thickness-to-chord ratio, and vertical offset. The lowest observed configuration (Fig. 7) shows a high vertical offset with a low t/c ratio. The lowest fitted configuration (Fig. 6) shows a zero vertical offset with a high t/c ratio. These two variables are strongly related. The buckling modes change significantly with variation of these two variables. In addition, the outboard wing sweep angle is at its upper bound for the lowest fitted configuration and it is highly forward swept for the lowest observed configuration.

Finally, the lowest observed and lowest fitted weight configurations were reanalyzed using a fully nonlinear analysis, including follower force effects, and were examined further by

Table 5 Optimal configurations determined from response surface

Parameter	First optimal	Second optimal	Third optimal
Front wing sweep angle	34.89 deg	30.00 deg	34.33 deg
Outboard wing sweep angle	60.00 deg	−22.36 deg	60.00 deg
Aft wing sweep angle	20.40 deg	19.52 deg	28.01 deg
Joint location	0.594	0.716	0.581
Vertical offset	0.0 m	10.0 m	0.0 m
Thickness-to-chord ratio	20%	10.60%	10.60%
First fitted half-wing weight	**−21006.6 kg**	−9490.09 kg	−9353.99 kg
Observed half-wing weight	4011.69 kg	**2913.16 kg**	4363.23 kg
Second fitted half-wing weight	2141.93 kg	**1314.37 kg**	3551.92 kg

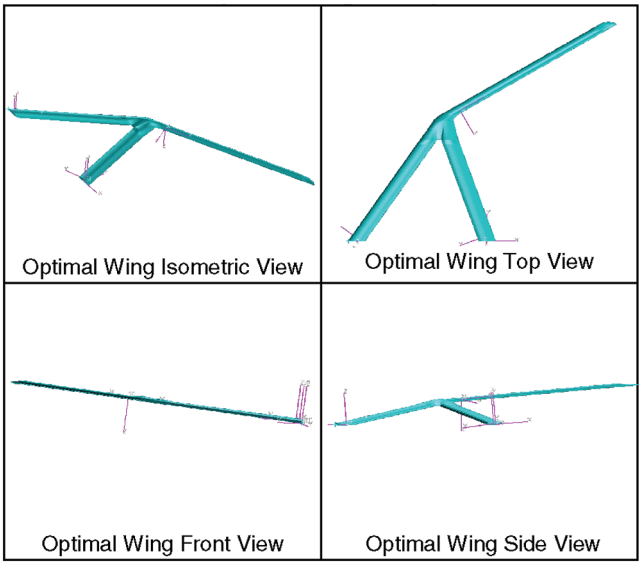

Fig. 6 Various views of the lowest fitted (first optimal) configuration.

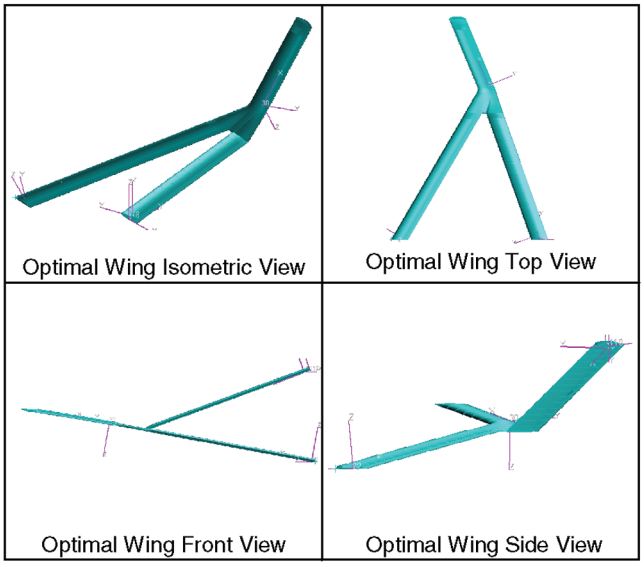

Fig. 7 Various views of the lowest observed (second optimal) configuration.

looking at their buckling modes, aerodynamic distributions, and material distributions.

B. Buckling Modes

There is a tradeoff between the vertical offset and thickness-to-chord ratio. As discussed before, the two configurations of interest show a high vertical offset with a low airfoil t/c ratio or a low vertical offset with a high t/c ratio. This is caused primarily by the bending plane tilt due to the vertical offset [1]. An increase in airfoil thickness-to-chord ratio is required to increase the bending moment of inertia when the front and aft wings are in the same plane.

The configuration with the low vertical offset can still be buckling critical. As Table 6 suggests, the first optimal (lowest fitted) configuration displays numerous local panel buckling modes. For the second optimal (lowest observed) configuration, a majority of the critical buckling loads correspond to global buckling modes. This shows that a vertical offset can induce aft wing buckling, whereas panel buckling becomes the critical buckling load for no vertical offset.

The total joined-wing finite element model contained 4722 elements. The total finite element model was accurate in representing

Table 6 Lowest buckling mode value for each load case before optimization

Load case	First optimal (Fig. 6) critical eigenvalue	Second optimal (Fig. 7) critical eigenvalue
2.5 G maneuver (mission start)	0.5429 (local)	0.4359 (local)
2.5 G maneuver (mission end)	(local)	1.1015 (global)
Turbulent gust	(local)	1.9564 (global)
Taxi impact	(local)	1.9618 (global)

global buckling. Conversely, the skin panels contained an average of 49 elements each. Panel buckling was observed, but a higher resolution panel buckling model should be added to the optimization to fully realize accurate panel buckling eigenvalues.

C. Aerodynamic Distributions

Figures 8–10 show the spanwise aerodynamic distributions of a 2.5 G pull-up maneuver load case for the lowest observed (second optimal) configuration. The front wing shows a traditional elliptical profile. The joined-wing model uses an aft wing twisting mechanism to control the aircraft pitch. This mechanism changes the angle of attack across the aft wing characteristic of longitudinal torsion. The aft wing shows a reverse elliptical profile because of this control mechanism. The joint wing section shows a large amount of lift

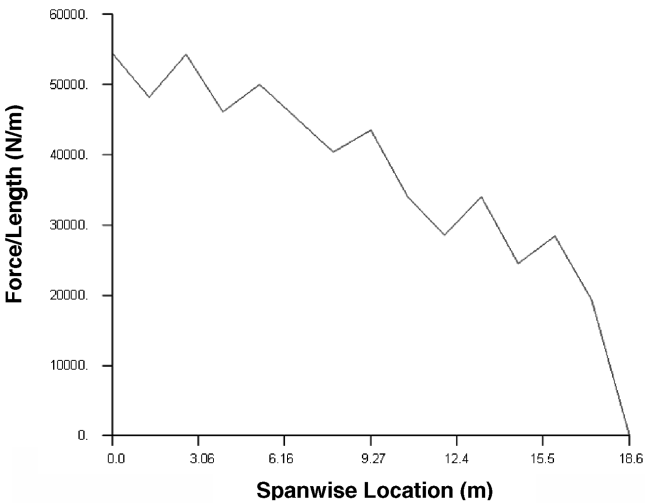

Fig. 8 Aerodynamic distribution on the front wing for the lowest observed configuration.

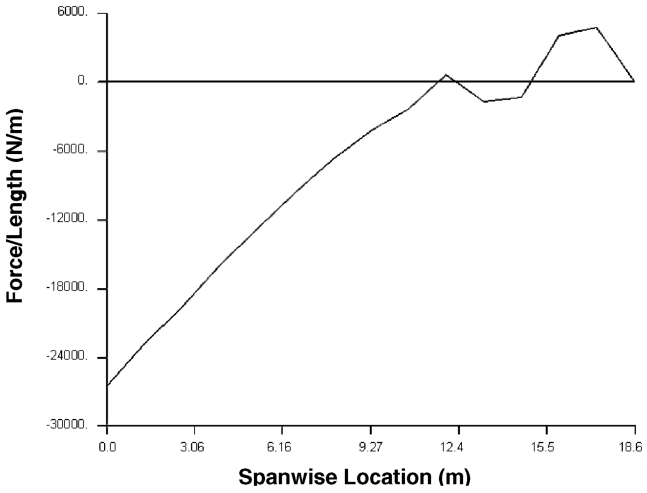

Fig. 9 Aerodynamic distribution on the aft wing for the lowest observed configuration.

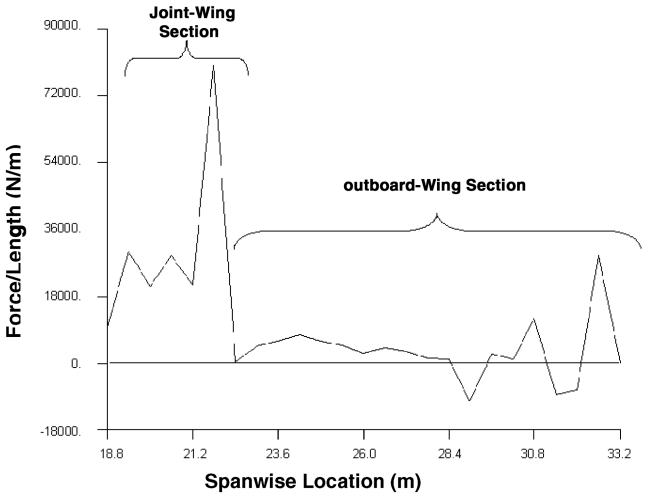

Fig. 10 Aerodynamic distribution on the joint/outboard wing for the lowest observed configuration.

whereas the outboard wing distribution is more flat and uniform across the outboard wing distance.

The aerodynamic distribution plots display jagged running loads due to a low number of spline point locations. Spline locations were placed only on the top of the substructure. More spline locations were placed on the ribs than on the spars. Smoother spanwise load distributions are possible with spline locations everywhere across the entire wing rather than isolated to the joined-wing substructure. The spike in the load profile at the joint and outboard wing juncture indicates the need to improve the airfoil design at the joint.

The low outboard wing load distribution occurs from aeroelastic tailoring. The outboard wing has thick 45 deg / − 45 deg plies that cause favorable bending-twist coupling. This decrease in wing twist with up-wing bending, even though it is forward swept, gives a lower incidental angle of attack for the outboard wing and a lower aerodynamic distribution.

D. Material Distribution

Figure 11 shows the material distribution for the lowest observed weight joined-wing configuration for 0 deg ply orientations in the skin. The lowest observed (second optimal) joined-wing configuration has a high vertical offset. The optimal material placement for a joined wing with a high vertical offset is at the forward-top skins and the rear-bottom skins. This resists longitudinal bending moments due to the front and top parts of the wing box being the furthest distance from the bending plane neutral surface [2].

The lowest fitted (first optimal) joined-wing configuration has no vertical offset. To resist bending, the optimal material placement is in the top and bottom skins. This follows conventional wing box design. This is revealed in Fig. 12 where the material is thick across the top skins and bottom (not shown) skins.

Even though the modified first optimal unswept outboard wing and second optimal configurations have very different vertical offset characteristics, they both exhibited relatively low weight values (2920 and 2913 Kg, respectively). This shows that the configuration with the high vertical offset resists bending well, while still preventing global buckling in the aft wing. The converse is also true. The configuration with no vertical offset does not geometrically resist bending well, but it resists global buckling well.

Aeroelastic tailoring was present in the outboard wing of the second optimal configuration. The outboard wing would twist down for an upward bending on a forward swept wing. The 45 deg plies were found to be much thicker than any other ply orientation. This provided the favorable bending-twist coupling.

Fig. 11 Top view (left) and bottom view (right) of material distribution for 0 deg ply orientation on the lowest observed (second optimal) configuration.

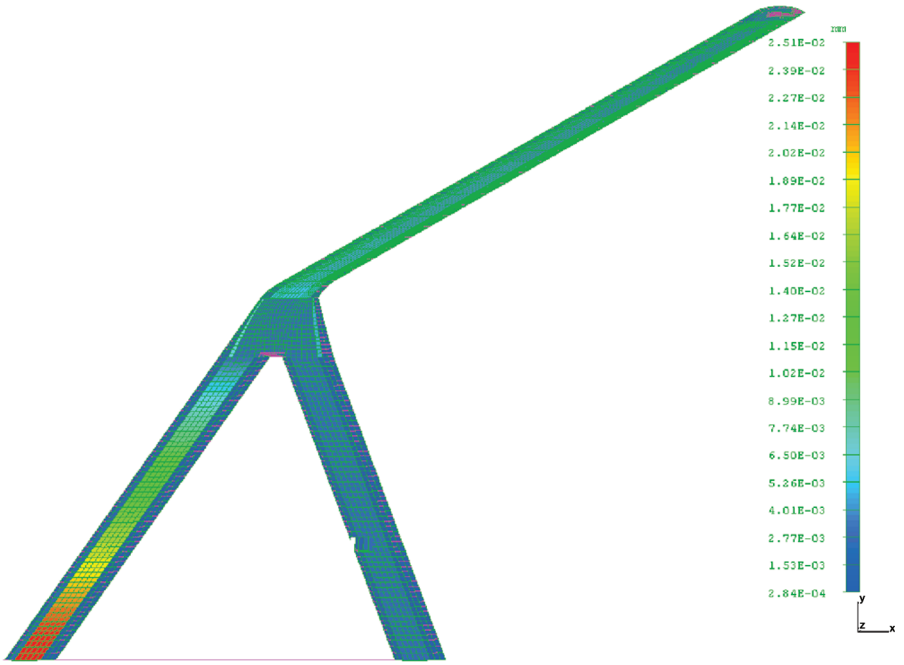

Fig. 12 Top view of material distribution for 0 deg ply orientation on the lowest fitted (first optimal) configuration.

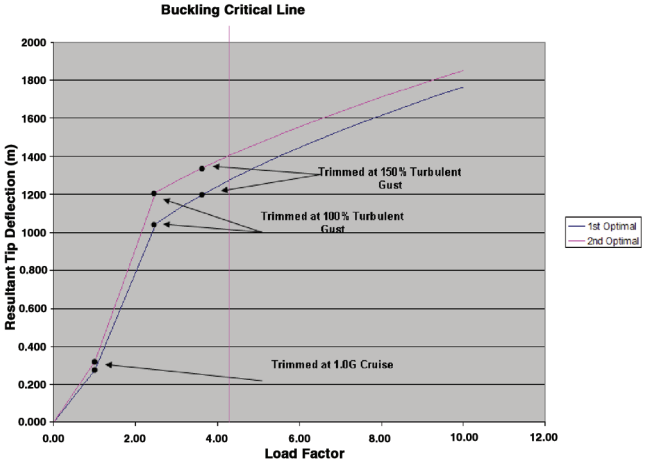

Fig. 13 Nonlinear Deflections of a turbulent gust load case.

E. Nonlinear Verification

Nonlinear analysis was conducted on the lowest observed and lowest fitted weight configurations. The quasistatic loads were taken from three separate points in the midst of a turbulent gust. The first trim case was a 1.0 G straight-and-level cruise condition. The second case was taken at 100% of a turbulent-gust condition where the change in angle of attack was calculated from a vertical gust wind velocity, Eq. (1). The third case was taken at 150% of the turbulent-gust condition. The forces at different load conditions can provide nonlinear aerodynamic changes for a gust load case.

Figure 13 shows the wing tip deflection with respect to the load factor. The tip deflections at the three calculated load conditions are shown as black dots. The buckling critical load for the lowest observed weight configuration is shown as a vertical line. The aerodynamic forces change nonlinearly from a 1.0 G cruise case to a 100% turbulent gust. The tip deflections occurring after this point show only structural stiffening instead of softening.

V. Conclusions

There is a vertical offset tradeoff represented in the joined-wing concept. The wing either tends towards a high vertical offset, which resists wing bending at a low t/c, or it tends toward a low vertical offset with a high t/c, which is a more traditional in-plane wing configuration. An interesting note is that a low thickness-to-chord ratio can produce a lighter weight aircraft than a large thickness-to-chord ratio due to the vertical offset. If there is no vertical offset, the wings are in plane and panel buckling becomes critical, rather than global wing buckling. A panel buckling model should be included if joined-wing configuration optimization continues.

The configurations listed in Table 5 showed that all optimal front and aft wing sweep angles reside at a configuration that produces a 360 deg radar coverage. Additionally, the fitted and observed weights show a substantial difference. This demonstrates that the response surface must be adaptively refined around the local optimal regions, if a true optimal joined-wing configuration is to be found.

A smoother aerodynamic distribution would be beneficial to the joined-wing optimization. This would provide a more realistic aerodynamic pressure distribution chordwise and spanwise across the wing. A higher number of spline locations in the FlightLoads model would generate a better distribution.

Nonlinear structural and aerodynamic effects, especially for a gust load condition, should be accounted for in joined-wing optimization and analysis. Obtaining new load sets at different flight conditions and at different load factors for each flight condition is required to truly model the aeroelastic effects of the joined wing throughout its mission profile.

Acknowledgements

The Air Force Office of Scientific Research funded this research. The authors gratefully acknowledge the support of the computational mathematics program manager, Fariba Fahroo.

References

[1] Rasmussen, C., Canfield, R., and Blair, M., "Optimization Process for Configuration of Flexible Joined-Wing," AIAA Paper 2004-4330, 2004.

[2] Wolkovich, J., "The Joined Wing: An Overview," *Journal of Aircraft*, Vol. 23, No. 3, 1986, pp. 161–178.

[3] Gallman, J. W., and Kroo, I. M., "Structural Optimization for Joined-Wing Synthesis," *Journal of Aircraft*, Vol. 33, No. 1, Jan.–Feb. 1996, pp. 214–223.

[4] Raymer, Daniel P., *Aircraft Design: A Conceptual Approach*, AIAA Education Series, AIAA, Reston, VA, 1999.

[5] Smith, S. C., Cliff, S. E., and Kroo, I. M., "The Design of a Joined-Wing Flight Demonstrator Aircraft," AIAA Paper 87-2930, 1987.
[6] Kroo, I. M., Gallman, J. W., and Smith, S. C., "Aerodynamic and Structural Studies of Joined-Wing Aircraft," *Journal of Aircraft*, Vol. 28, No. 1, Jan.–Feb. 1991, pp. 74–81.
[7] Gallman, J. W., Kroo, I. M., and Smith, S. C., "Optimization of Joined-Wing Aircraft," *Journal of Aircraft*, Vol. 30, No. 6, Nov.–Dec. 1993, pp. 897–905.
[8] Lin, H-H., Jhou, J., and Stearman, R., "Influence of Joint Fixiti on the Aeroelastic Characteristics of a Joined Wing Structure," *Proceedings of the 31st AIAA/ASME/ASCE/AHS/ASC Structures, Structural Dynamics and Materials Conference*, AIAA, Washington, D.C., April 1990, pp. 1442–1454; also AIAA Paper 90-0980.
[9] Livne, E., "Aeroelasticity of Joined-Wing Airplane Configurations: Past Work and Future Challenges—A Survey," AIAA Paper 2001-1370, 2001.
[10] Blair, M., and Canfield, R., "A Joined-Wing Structural Weight Modeling Study," AIAA Paper 2002-1337, 2002.
[11] Roberts, R., Canfield, R., and Blair, M., "Joined-Wing Aeroelastic Design with Geometric Nonlinearity," *Journal of Aircraft*, Vol. 42, No. 4, July–Aug. 2005, pp. 832–848.
[12] Weisshaar, T., and Lee, D., "Aeroelastic Tailoring of Joined-Wing Configurations," AIAA Paper 2002-1207, 2002.
[13] Nangia, R. K., and Palmer, M. E., "Unconventional High Aspect Ratio Joined-Wing Aircraft with Aft and Forward Swept Wing Tips," AIAA Paper 2003-0506, 2003.
[14] "Adaptive Modeling Language Basic Training Manual: Ver. 2.07," TechnoSoft Incorporated, 2001.
[15] "MSC.NASTRAN Ver. 68 Reference Manual," MacNeal-Schwendler Corporation, 1995.
[16] Schwartz, J., Canfield, R., and Blair, M., "Aero-Structural Coupling and Sensitivity of a Joined-Wing SensorCraft," AIAA Paper 2003-1580, 2003.
[17] "MSC/NASTRAN Aeroelastic Analysis," MacNeal-Schwendler Corporation, 1994.
[18] Rasmussen, C., "Optimization Process for Configuration of Flexible Joined-Wing," M.S. Thesis, AFIT/GAE/ENY/04-M14, Graduate School of Engineering Air Force Institute of Technology (AETC), Wright–Patterson AFB OH, March 2004.
[19] Lan, C. T., and Roskam, J., *Airplane Aerodynamics and Performance*, 2nd ed., AIAA, Washington, D.C., 1992.
[20] "MATLAB Reference Guide: Ver. 6.1," The MathWorks, Inc., 2001.